

Influence of tilt and surface roughness on the outflow wind field of an impinging jet

M.S. Mason*

School of Civil Engineering, University of Sydney, NSW, Australia

G.S. Wood

Cermak Peterka Petersen, St. Peters, NSW, Australia

D.F. Fletcher

School of Chemical and Biomolecular Engineering, University of Sydney, NSW, Australia

(Received August 9, 2008, Accepted January 30, 2009)

Abstract. A physical and numerical steady flow impinging jet has been used to simulate the bulk characteristics of a downburst-like wind field. The influence of downdraft tilt and surface roughness on the ensuing wall jet flow has been investigated. It was found that a simulated downdraft impinging the surface at a non-normal angle has the potential for causing larger structural loads than the normal impingement case. It was also found that for the current impinging jet simulations, surface roughness played a minor role in determining the storm maximum wind structure, but this influence increased as the wall jet diverged. However, through comparison with previous research it was found that the influence of surface roughness is Reynolds number dependent and therefore may differ from that reported herein for full-scale downburst cases. Using the current experimental results an empirical model has been developed for laboratory-scale impinging jet velocity structure that includes the influence of both jet tilt and surface roughness.

Keywords: Downburst; microburst; impinging jet; tilted jet; surface roughness; empirical model.

1. Introduction

Downburst wind events are of importance to engineers because in many parts of the world they are responsible for the wind gusts used for wind resistant design (Gomes and Vickery 1976, Holmes 2002, Twisdale and Vickery 1992). What is known of the structure of these events is largely based on a series of observational studies conducted during the 1970s and 80s (Fujita 1985, 1990, Hjelmfelt 1988, Wilson, *et al.* 1984), and more recent work designed for engineering consumption (Choi 2004, Holmes, *et al.* 2008, Orwig and Schroeder 2007). From the earlier works, Hjelmfelt

* Corresponding Author, E-mail: m.mason@usyd.edu.au

(1988) drew a comparison between the normalised structure of downburst outflows and a steady flowing laboratory scale impinging jet. Although modelling downburst winds using a steady impinging jet neglects some important atmospheric and physical parameters (e.g. non-stationarity, gust front structure), it has proven to be a reasonably simple and useful tool for understanding the general kinematics of these events (Letchford, *et al.* 2002). To this end, the steady flowing impinging jet will be used to investigate two outflow parameters that have received little attention, downdraft/jet tilt, and surface roughness. The results of these investigations are used to further develop an empirical model for predicting impinging jet flow. As well as the steady flowing impingement case modelled, it is believed that the findings of the current study provide a good indication of flow behaviour likely to occur during unsteady downburst events.

Fujita (1985) describes the downburst not as a single type of outflow event, but as a family of storm outflows that originate aloft and descend to, then diverge along, the ground. For this reason it is important to not only investigate the simple normal impingement case, but to investigate other possible outflow scenarios so that a “worst case” outflow structure can be determined. In this study the influence of the angle of jet tilt on the structure of the outflow is investigated. The need for this type of study is exemplified by Fujita’s analysis of a series of microburst wind events that occurred during the JAWS monitoring project in 1982, Fig. 1. During this event each of the microbursts approached the ground at non-normal angles, an impingement scenario not typically considered by wind engineering researchers. Hjelmfelt (1988) and Proctor (1993) discuss the occurrence of non-normal impingement, and suggest that a tilted downdraft core may occur when momentum from surrounding flow is transferred to the downdraft column. Hjelmfelt (1988) concludes that this transfer of momentum does little to change the morphology of the downdraft, and that superposition of the ambient winds and a normal impinging downdraft adequately explains the resulting flow patterns. Probably the most prominent case of a tilted downburst is the Andrews Air Force Base microburst that is reported to have had a jet tilt (from normal) of approximately 23° (Fujita 1983) and a recorded gust wind speed of 67 m/s at an elevation of 5 m. The occurrence of such an event highlights that not only do these events occur, but the magnitude they can reach is of concern to ultimate wind resistant design. Initial work on the importance of downdraft descent angle (Mason and Wood 2005) has shown the simulated downdraft angle influences the overall drag on small model cubes placed at different positions within the simulated outflow. This earlier work did not endeavour to investigate the structure of the velocity field causing this loading.

A second parameter that has received relatively little attention is the importance of surface roughness in the development of wind structure as a simulated outflow spreads over an impingement surface. Whittingham (1964) suggested that surface roughness plays a minor role in the velocity structure of a thunderstorm outflow near peak intensity. This was primarily believed because the outflow itself would not have been in contact with the rough ground for long enough to allow the

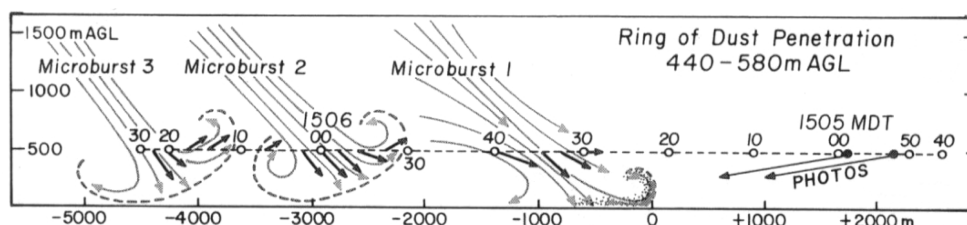


Fig. 1 Analysis of a series of microbursts in Watkins, Colorado during the JAWS monitoring project (Fujita 1985)

full extent of mechanical turbulence to influence the flow prior to storm peak. Proctor (1988) on the other hand, through use of a mesoscale numerical model, shows that surface roughness plays an important role in development of the gust front leading the outflow. For an impinging jet, Xu and Hangan (2008) and Choi (2004) have studied the influence surface roughness has on the height and magnitude of the maximum velocity for a range of Reynolds numbers and impinging jet to surface distances. These data show that for all test cases increasing surface roughness increases the elevation of maximum winds, and decreases the magnitude of these winds.

The current study investigates the two impinging jet parameters, jet tilt and surface roughness, and discusses their importance to downburst modelling. The results are used to build an empirical model to describe the velocity profile of impinging jet outflows in the near-impingement region. The impinging jets are studied both experimentally and numerically, with the numerical results being used where experimentation proved impractical.

2. Test setup

2.1. Experimental setup

Experimentation was undertaken at the School of Civil Engineering Impinging Jet Facility within The University of Sydney, Fig. 2. The facility has a 0.104 m diameter, D , circular plastic pipe which runs uninterrupted for 6 m and expels air onto an impingement surface 0.208 m from the outlet; as measured along the jet centre line. This spacing approximates the *average* distance between ground and cloud base found during the JAWS project (Hjelmfelt 1988). The length of pipe is sufficient to obtain fully-developed velocity and turbulence profiles as determined by comparison with experiments by Laufer (1954). The jet was run so the spatially averaged velocity, w_{bulk} , through the pipe was 10 m/s ($Re = 70,000$) with a centre-line mean velocity, w_{cl} , measured at the jet outlet, of approximately 12 m/s. The impingement surface was able to be rotated around the y -axis, Fig. 2 (b), so the incidence angle of the jet to the surface could be varied. The measure of jet to surface incidence is expressed throughout this paper as an angle of jet tilt, θ , defined by $\theta = x'/z' = \tan(\gamma)$, Fig. 2 (b), and is a measure of the tilt angle from normal impingement. The set of jet tilts tested were $\theta = 0, 0.125, 0.25, 0.5$ and 0.7 , which correspond to angles of $\gamma = 0^\circ, 7^\circ, 14^\circ, 27^\circ$ and 35° . For

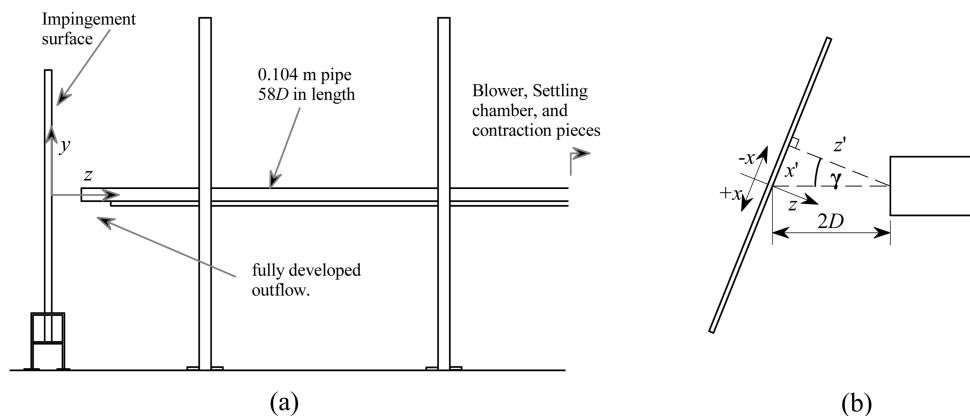


Fig. 2 Schematic diagram of the experimental impinging jet test facility (a), and (b), plan view schematic of a tilted jet test setup

smooth surface simulations, the impingement surface was covered with galvanised sheet metal to achieve a hydraulically smooth surface. For the rough surface tests differing grades of sandpaper were glued to a backing board, and then screwed to the impingement surface to simulate surfaces with a range of roughness characteristics. The roughness characteristics of each sandpaper were defined by the average size of the embedded particles, h_s . Particle sizes for each sandpaper were initially taken from ISO 6344-1 (International Organisation for Standardization 1998), and then tested in a boundary layer wind tunnel for velocity profile deformation. It was found that to a general approximation, the particle sizes matched those specified by ISO 6344-1, thus these sizes were used. The particular sandpaper grits used for the current tests were P120, P60, and P40, which corresponded to particle sizes of $h_s = 125, 269, \text{ and } 425 \mu\text{m}$. Throughout the paper these roughness levels are normalised against the jet diameter, D , leading to roughness values of $h_s/D = 0.0012, 0.0026, \text{ and } 0.0041$, respectively. All elevation measurements had a roughness correction equal to $h_s/2$ added to them because it was not possible to measure to the base of the sandpaper. A value of h_s was considered too large because the measurement device (ruler with 0.5 mm resolution) settled into the roughness elements themselves.

Mean velocity and turbulence kinetic energy, k , profiles were measured with a Turbulent Flow Instrumentation 4-hole 123 cobra probe and a single hot-wire anemometer sampled at 1250 Hz for 30 s. Velocity and turbulence comparisons between the cobra probe and the hot-wire anemometer showed the cobra probe to be suitable for use down to 2 mm (measured to the centre of the probe) from the surface. Below this point the hot-wire anemometer was used to measure the velocity fields so that a measure of the near-surface region could be made. The cobra probe however, was used where possible (i.e. $z > 2 \text{ mm}$) because it measured velocity fluctuations in three dimensions, which allowed an experimental measurement of k . The accuracy of the cobra probe is 0.2 m/s within the range 2 m/s – 30 m/s (Mousley 2002). The accuracy of the mean velocity readings in the lower part of the profile are expected to be within 4% of their true value. Additionally, errors in the given measurements will arise due to positioning and an averaging error over the faces for the cobra probe. These errors vary throughout the test domain, primarily caused by the variable velocity gradients over the region of measurement. Hot-wire measurements are expected to have an accuracy of approximately 2%, again with an elevation specific positioning error on top. The turbulence kinetic energy, since only measured by the cobra probe, has a corresponding expected accuracy to within $\pm 14\%$.

Mean velocity and k profiles were measured over the range $0.65 \leq x/D \leq 2.0$ for all rough surface configurations and $-2.0 \leq x/D \leq -0.8$, for the tilted jet tests where possible. Unfortunately the rig setup did not allow a full range of measurements in the tilted jet rear outflow ($x/D < 0$), but those taken have been used to validate the numerical predictions. From an ultimate design perspective, the velocity and turbulence structure to the rear of the jet are less important than those measured at the front, because these wind fields have reduced potential loading capacity. In general, tests were carried out as isolated investigations (i.e. tilted jet tests did not include any surface roughness and vice versa), however a number of bi-variate tests were conducted to validate the empirical function formulation. The process for acquiring these bi-variate results was identical to that just described except profiles were only measured at $x/D = 1.0$ and 2.0 .

2.2. Numerical setup

Mason, *et al.* (2007) found that numerical simulation was a valid method for predicting the

velocity, and (to a lesser extent) turbulence fields of a normal axi-symmetric impinging jet. This method was therefore used to simulate impinging jet flow for both the tilted jet and rough surface cases described above. Numerical simulations have been conducted for all jet tilt and rough surface configurations discussed in section 2.1. The numerical simulation results served to “fill the gaps” where experimentation became impractical, and to test the numerical model’s capabilities in these varying flow regimes.

All numerical simulations were carried out with the commercial CFD solver, ANSYS CFX11 (ANSYS 2007), which is a finite volume solver for the mass and momentum (and energy if required) equations. The numerical scheme is a co-located pressure based method that utilises a modified Rhie-Chow algorithm to avoid decoupling. The resulting algebraic equations are solved by an algebraic multi-grid method. All velocity calculations use a second order bounded differencing scheme, while for reasons of stability a first order upwind scheme is implemented for the convective terms in the turbulence equations. A second order scheme is used for all diffusive terms.

As with the experimentation, the numerical simulations modelled a stationary, steady flow, impinging jet with a jet Reynolds number of approximately 70,000. To include the influence of jet tilt a mirrored three dimensional domain was used, Fig. 3 (a). The numerical domain utilises the centre-line symmetry of the flow and simulates half of the impinging jet outflow using a tilted half-cylinder of diameter $8D$, and axial length of $2.5D$. The exact shape of the domain was dependent on the jet tilt simulated. The jet outlet was set at $z/D = 2$ above the impingement surface, as measured along the jet centre line. In all cases a y^+ value less than 1.0 is maintained and the domain is essentially divided circumferentially into 1.3° slices of a radial 170×270 grid. For the rough surface simulations, the wall normal orientation of the jet meant that 3D simulations were unnecessary. For these simulations a 2D axi-symmetric domain with an axial length of $2.5D$, and radial dimension of $5D$ was used, Fig. 3 (b). The domain was divided into a non-isotropic 400×400 grid with y^+ values not exceeding 1.0. The automated wall treatment feature of ANSYS CFX11, which shifts the wall to an elevation of $h_s/2$ to avoid developing the boundary layer within the roughness elements, allowed the use of a single mesh for all roughness cases. The use of the 2D axi-symmetric domain was a computational time saving strategy, and comparison between 2D axi-symmetric and 3D simulation results revealed no significant differences in the velocity or turbulence structure. Both types of simulation used hexahedral mesh elements and the above specifications were found to be insensitive to mesh refinement when assessing velocity and k profiles.

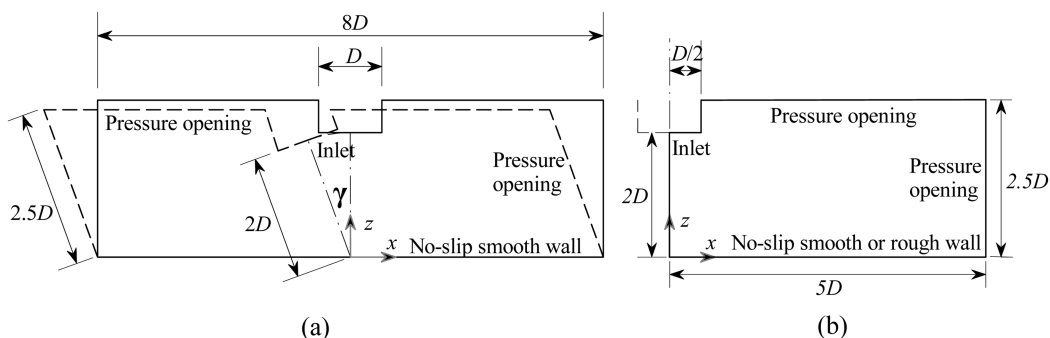


Fig. 3 Numerical geometry and boundary conditions for (a) tilted jet simulations, and (b) rough surface simulations

Mean velocity, turbulence kinetic energy, k , and turbulence energy dissipation, ε , were set at both domain inlets, Fig. 3. The velocity and k values were measured experimentally at the jet outlet, while ε values were taken from a separate fully-developed numerical pipe flow simulation because of the experimental difficulty in measuring this value. The top and side boundaries were set as pressure openings that allow flow to enter or leave the domain based on an assigned relative pressure (zero in this case). The mirror face of the 3D domain and the two side faces of the axisymmetric domain were set as symmetry boundaries. The ground was treated as a no-slip smooth wall for tilted jet simulations, and as a no-slip rough wall for the wall roughness simulations. The near wall treatment for the no-slip smooth wall cases is as described in Mason, *et al.* (2007) where a low Reynolds number formulation allows behaviour in the laminar sub-layer to be incorporated into the calculation of values at the near-wall node. For the rough surface simulations, a roughness dependent formulation of the near wall node values allows for the laminar sub-layer to be included in calculations when not destroyed by the roughness itself. The near-wall velocity characteristics are calculated based on the viscous sub-layer formulation for the smooth wall shear velocity, u_τ :

$$u_\tau = \sqrt{\frac{\mu \partial u}{\rho \partial z}} \quad (1)$$

corrected to account for the rough wall behaviour via a multiplication factor based on the rough and smooth wall formulations of u_τ in the log layer (White 1991). Further information on this adjustment can be found in Mason (2009).

Mason, *et al.* (2007) studied a series of turbulence closure schemes available in CFX11.0, and assessed the applicability of each for modelling impinging jet flow. It was found that from the RANS models available, the Shear Stress Transport (SST) closure performed the best in predicting both velocity and turbulence profiles for $x/D < 2.0$. The SST closure is applied for all numerical simulations in this paper.

3. Results and discussion

The flow structure of a surface-normal round impinging jet is relatively well documented because of its application to a wide range of industries (e.g. heating/cooling, drying, aircraft take-off, pollution dispersion) (Knowles and Myszko 1998, Xu and Hangan 2008), and of course wind engineering applications (Chay and Letchford 2002, Mason, *et al.* 2007, Sengupta and Sarkar 2008). From these works it is evident that although the general flow structure remains the same for all impinging jets, characteristics such as Reynolds number and jet outlet to impingement surface distance can significantly influence the flow structure at a given location. Flow changes are particularly prevalent in the impingement region, i.e. prior to self similarity, $x/D < 3.0$ (or 4.5 if considering turbulence profiles) (Knowles and Myszko 1998). Bearing this in mind, the flow described throughout this section details simulations using a single impinging jet, run at a single Reynolds number, and single jet to surface spacing. Therefore the exact numbers presented may vary from jet to jet, and indeed in the extension to a full-scale downdraft, but the principles are expected to remain the same for all applications.

Section 3 is split into four parts. Section 3.1 describes the base simulation, i.e., normal impingement ($\theta = 0$) and smooth surface ($h_s/D = 0$), to which all other simulations are compared. Section 3.2 discusses the tilted jet simulations. Section 3.3 discusses the rough surface simulation results. Section 3.4 uses the results given in sections 3.1 - 3.3 to build an empirical model of the impinging jet wind speeds for the range of jet tilt and surface roughness parameters tested.

3.1. Normal impingement, smooth surface case ($\theta = 0, h_s/D = 0$)

The normal impingement, smooth surface case describes the flow structure for the model parameters, $\theta=0, h_s/D=0$. This flow case produces the velocity and turbulence structure from which the tests described in the following two sections will deviate.

Fig. 4 (a) shows normalised mean u velocity profiles plotted against normalised height z/D , where u is the velocity component parallel to the impingement surface, w_{cl} is the mean jet centre-line velocity, z is the elevation measured from and normal to the surface, and D is the jet diameter. This referencing system will be used throughout this paper. It is evident for all profiles that the normalised mean velocity reaches a maximum close to the surface, $z/D < 0.02$, and decays with increased elevation above this point. Profile shapes are seen to change significantly through the region $x/D \leq 1.0$, but then remain relatively constant. The flow field is seen to increase to an overall simulation maximum velocity, u_{storm} , at $x/D \approx 1.0$, after which point the maximum velocity recorded at each radial position, u_{max} , decreases for increased divergence from the jet. This behaviour is similar to that reported for full-scale downburst winds (Hjelmfelt 1988). Mean velocity profiles predicted by the numerical model are seen to be in good agreement with the experimentally measured profiles at all locations, particularly in the region $z/D < 0.1$. This level of agreement means that the numerical model can be used to supplement experimental mean velocity results where these were physically unable to be taken.

Fig. 4 (b) shows the turbulence kinetic energy, $k = 1/2(u'^2 + v'^2 + w'^2)$, structure at the same radial locations discussed for Fig. 4 (a). u', v', w' are the statistical velocity fluctuations about the mean values u, v, w in the x, y, z , directions, respectively. Values of turbulence kinetic energy are normalised by the square of the mean jet centre-line velocity, w_{cl} . Experimental k values are shown only for $z/D > 0.02$, where the Cobra Probe could be used. The single hot-wire measurements were unable to measure the three components of the fluctuating velocity and therefore were unable to produce values of k . When discussing the wall parallel component of turbulence, u' , Xu and Hangan

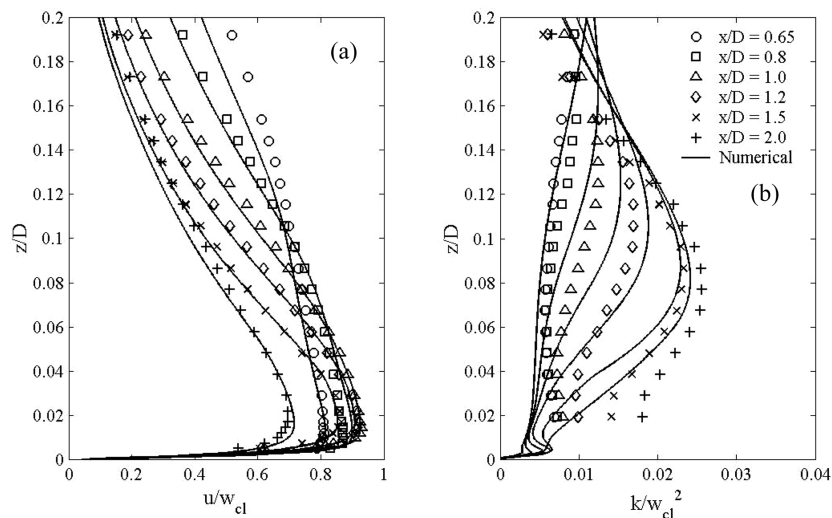


Fig. 4 Normalised velocity, (a), and turbulence kinetic energy, k , (b), profiles for $0.65 \leq x/D \leq 2.0$, for the baseline experiments and numerical simulations

(2008) describe profiles with two maxima, one in the “inner layer” associated with the wall shear (approximately at or below the velocity maxima), and a second in the “outer layer” (above the velocity maxima) associated with the interaction between the free jet and the developing boundary layer. These regions effectively correlate to the “in-boundary layer”, and “out-of boundary layer” regions described in the empirical model formulation of Oseguera and Bowles (1988) discussed in section 3.4. The same structure is evident in the current experimental results shown in Fig. 4 (b), but due to the inability of the cobra probe to measure in the $z/D < 0.02$ region the inner layer peak is not well defined. All profiles do however indicate movement towards these maxima. Inspecting the numerical results it is seen that the quality of fit to the experimental data is not as good as for the mean velocity profiles, but is generally good in the outer layer. For this outer layer the decreasing trend in elevation of the maxima is well predicted by the numerical model, as is the magnitude of the peak for many of the radial locations. For the inner layer it appears that the wall shear induced peak is under predicted in all cases, however this does not appear to adversely affect the velocity structure discussed for Fig. 4 (a). For the surface roughness simulations discussed in section 3.3, it will be shown that the under prediction of k in this region leads to inaccurate prediction of roughness perturbed velocity.

To the authors knowledge there is no available full-scale data for turbulence profiles through the depth of a downburst outflow, so no comment can be made on the general applicability of the impinging jet in this case. However, based on measurements from the rear flank downdraft recorded in Lubbock 2003, Chen and Letchford (2005) and Holmes, *et al.* (2008) suggest that near ground level, longitudinal turbulence intensities of approximately 10% exist. This value is approximately equal to those measured near the surface at $x/D = 1.0$ in the current experiments (based on u').

3.2. Tilted jet simulations

Little is known of the role downdraft tilt plays in the outflow structure of downburst wind events. To address this issue a series of tilted jet tests have been performed to investigate this parameter.

Fig. 5 shows the normalised mean velocity profiles measured at $x/D = \pm 1.0$ for each of the tilted jet, smooth surface, simulations. The region $x/D > 0$ is referred to as the “forward” side of the jet outflow, while $x/D < 0$ is referred to as the “rear”. From the results shown in Fig. 5 (b) it is evident that as jet tilt increases, so too does the forward wall jet thickness. This increase in thickness leads to mean velocity gradients above u_{max} comparatively decreasing when viewed against the $\theta = 0$ case. This progression suggests that as the jet tilt increases, the winds felt by a structure become more uniform with height, and larger loads are therefore theoretically applied to an impacted structure. It is however evident that although significant differences exist in the velocity magnitude at large elevations, only a relatively minor increase in the magnitude of u_{max} occurs for increased levels of tilt. For the rear side of the jet, Fig. 5 (a), the opposite is seen to occur, and it is evident that for each increase in jet tilt, a reduction in wall jet thickness is recorded. Through the concept of mass conservation, these findings suggest that as jet tilt is increased the flux balance is skewed towards the front of the jet with less flow directed rearward. This behaviour occurs because the stagnation region generally associated with a maximum at $x/D = 0$ progressively moves to larger negative x/D values.

In Fig. 5 (b) it is evident that as the jet tilt increases the numerical model slightly under predicts the velocity magnitude for $z/D > 0.1$, similar to that observed for the $\theta = 0$ case. To the rear of the jet, Fig. 5 (a), agreement is seen to be good, and it is assumed that for tests where experimental

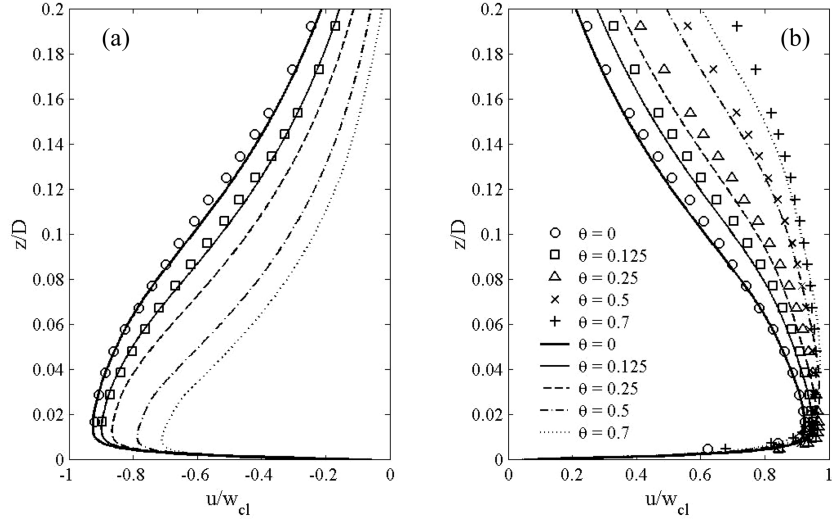


Fig. 5 Experimental and numerical normalised mean velocity profiles for the jet tilt range of $0 \leq \theta \leq 0.7$ at (a) $x/D = -1.0$, and (b) $x/D = 1.0$. Experimental results are shown as symbols, and numerical predictions are shown as lines

measurements were impractical this level of agreement would continue. For this reason numerical results were considered representative and much of the discussion to follow is based on the numerical predictions.

The general thickness of a wall jet is often described by the elevation to $u_{max}/2$ (above u_{max}), because normalisation by this height allows a full collapse of velocity profiles in the self-similar region (e.g. Knowles and Myszko 1998). This method of describing wall jet thickness is applied here through use of the length scale $\delta = z(u_{max}/2)$. Plotting δ/D with radial position and jet tilt, Fig. 6 shows the increasing δ trend with increasing θ discussed for Fig. 5 is maintained for much of the region $x/D < 2.0$. For the forward side of the jet outflow the results show a decreasing dependence on θ with increased x/D . It would however be unsurprising if there was some residual influence on mean velocity structure that extends further than the typical impingement zone because of the rearward shift of the stagnation zone.

It was noted earlier that at $x/D = 1.0$, Fig. 5 (b), there is only about 5% variability in the range of u_{max} . However, inspecting the dependence of u_{max} on jet tilt for the range $-2.5 \leq x/D \leq 2.5$, Fig. 7, it is clear that variability increases significantly away from this location. For the forward jet outflow region, it is seen that as the angle of jet tilt increases, the event maximum mean velocity, u_{storm} , also increases. Drift of the radial location of maximum velocity from the jet centre-line also occurs. The radial length over which high u_{max} values are maintained is seen to increase for larger values of jet tilt. The range of u_{max} values found for $0 \leq x/D \leq 1.0$ is shown to be greater than indicated by Fig. 5 (b) because the movement of the stagnation zone towards the rear of the jet means that u_{max} is not zero at $x/D = 0$, but maintains an increasing component of horizontal velocity for an increasing level of jet tilt. To the rear of the jet, the u_{max} structure appears to be less complicated and a distinct reduction in u_{max} for all radial location is observed for increased jet tilt. The peak rear side storm velocities are however confined to a single radial location, $x/D \approx -1.0$. The range over which the rearward u_{max} varies with respect to jet tilt is seen to be approximately constant over the entire radial range tested. The relationship between forward and rearward outflow characteristics reported

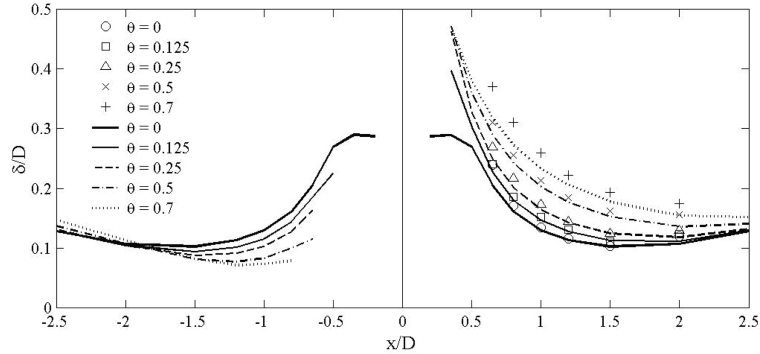


Fig. 6 Variability of wall jet thickness, δ , with respect to radial position and jet tilt. Experimental results are shown as symbols, and numerical predictions are shown as lines

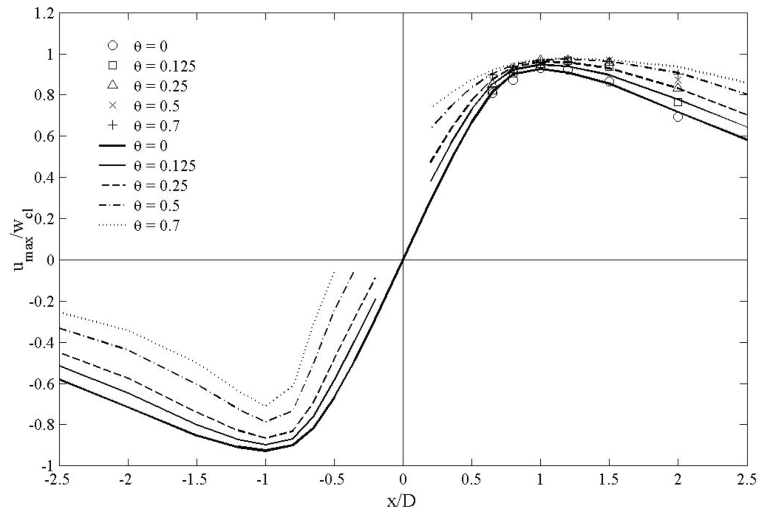


Fig. 7 Variability of maximum mean velocity, u_{max} , in the normalised velocity profile at each radial position for each jet tilt tested. Experimental results are shown as symbols, and numerical predictions are shown as lines

herein are similar to those found for tilted microbursts during the JAWS monitoring project (Wilson, *et al.* 1984).

Jet tilt also influenced the elevation of maximum velocity, z_{max} , Fig. 8. For both the forward and rear of the jet outflow, the behaviour of z_{max} with respect to jet tilt is similar to that shown for δ , Fig. 6. However, a simple evaluation of scale reveals that the range in z_{max} is generally smaller than that of δ and although the overall behaviour of z_{max} with respect to jet tilt is similar, the specific behaviour when viewed against radial position is not identical. This indicates that the flow ratio, z_{max}/δ , is dependent on θ . The importance of this parameter to the empirical model formulation is explained in section 3.4.

Inspecting the numerical predictions for the forward side of the jet outflow in Fig. 8, it is evident that for all jet tilts except $\theta = 0.5$ the numerical model performs well in predicting z_{max} . For $\theta = 0.5$, at several points the numerical model is seen to over predict the experimental value. However,

inspecting the corresponding mean velocity profile in Fig. 5, it is seen that over the region $0.02 \leq z/D \leq 0.06$ the velocity gradient is extremely small, which, when considering possible experimental error, makes location of an experimental z_{max} difficult. In fact, inspecting the experimental mean velocity at z_{max} elevations predicted by the numerical model reveals that these values are within 0.5% of u_{max} .

As well as the variability in mean velocity profiles, jet tilt was shown to induce variability in the turbulence kinetic energy profiles. Fig. 9 exemplifies the influence jet tilt has on k with a plot of profiles at $x/D = 1.0$ for each level of jet tilt. This location is the same as used in Fig. 5, and generally corresponds to the region near storm maximum velocity. For the forward side of the jet outflow, Fig. 9 (b), it is shown that associated with an increase in jet tilt is a rise in the elevation of the maximum k associated with the outer layer (section 3.1), and thus a decreasing k magnitude for elevations below this maximum when compared with the $\theta = 0$ case. Although not particularly clear in Fig. 9, the magnitude of this outer layer maximum was found to remain fairly constant (within 10-20%) with changes in θ . As with the normal impingement case, experimental results in the inner layer are tending towards a peak near the impingement surface, but are unable to be defined due to

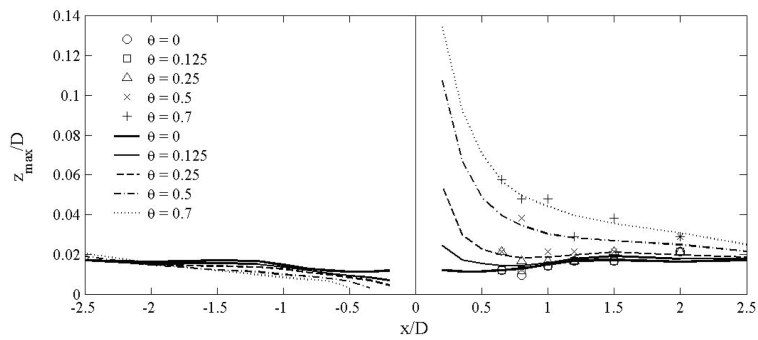


Fig. 8 Normalised elevation of maximum mean velocity. Experimental results are shown as symbols, and numerical predictions are shown as lines

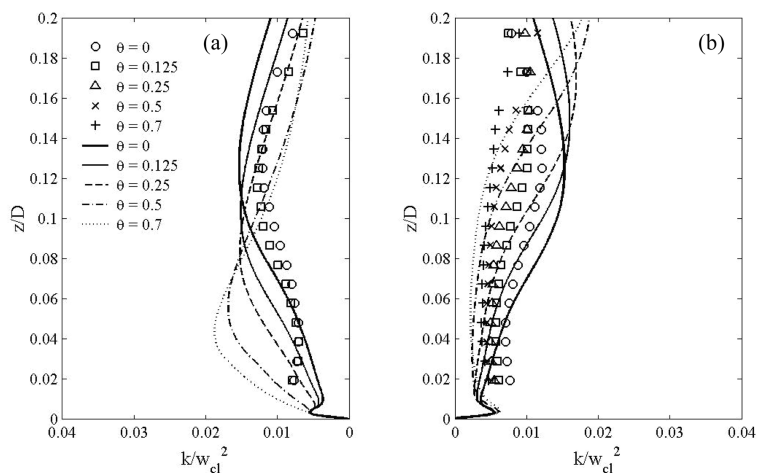


Fig. 9 Turbulence kinetic energy, k , profiles at (a) $x/D = -1.0$, and (b) $x/D = 1.0$, for the range of jet tilts tested. Experimental results are shown as symbols, and numerical predictions are shown as lines

the inability to measure k in this region. Numerical results in this region indicate that k is slightly increased in this layer. As the flow diverges this inner peak tends to become more defined, and the experimental results show this more clearly at these locations. The behaviour discussed for $x/D = 1.0$ is generally applicable for all measured radial positions.

Upon comparative inspection of Fig. 9 (a) and Fig. 6, it was found that δ values are directly proportional to the elevation of the outer layer peaks in the k profiles. Given this relationship, and recalling Fig. 6, it is not surprising that the elevation of this outer peak tends to decrease for increased θ on the rear side of the jet, Fig. 9 (a). For larger radial positions than shown, the outer peak moves with δ and is approximately constant for all tilt angles at $x/D = 2.0$, as observed in Fig. 6. Unlike for the forward side of the jet, the maximum magnitude of k to the rear was found to be dependent on θ when tilt is large. It was found that as the mean velocity gradient through the outer layer of the flow reduced, the maximum magnitude of k decreased. This behaviour is evident when comparing Fig. 9 (a) with Fig. 6 (a) at the elevations of maximum k ; this behaviour is however more predominant at larger radial locations where more of a difference is found in the mean velocity gradients.

Similar discrepancies between experimental and numerical results are noted in Fig. 9 (b) when compared with the normal impingement case, Fig. 4 (b). Similar numerical accuracy is found for all radial locations.

It is evident when considering the location of maximum potential loading for each of the tilted jet downburst simulations, the general influence of jet tilt on the mean velocity profile is to decrease the velocity gradient above u_{max} , thus increasing the potential load on a tall structure (say $z_{structure} = 0.1D$). This increase in potential load is achieved without a significant increase in maximum velocity and is driven primarily by the differing velocity decay gradients. At this same location it could also be expected that turbulence levels at a given height will be reduced as the angle of jet tilt increases, provided $z_{structure}$ is less than approximately $0.12D$ (the outer layer maximum for the normal impingement case).

3.3. Rough surface simulations

Surface roughness plays an important role in determining both the magnitude and structure of the mean velocity and turbulence profiles in boundary layer winds. It is therefore important to determine whether roughness plays as significant a role in determining these profiles during downburst events. To this end, this section details results of surface normal, $\theta = 0$, steady impinging jet simulations for flow diverging over rough surfaces. In their recent paper, Xu and Hangan (2008) discuss the role surface roughness plays in the development of u_{max} and z_{max} along an impingement surface for a range of impinging jets. The current tests complement this work and discuss the development of the wall jet thickness, δ , so that these parameters can be used for empirical model development.

The normalised mean velocity profile is shown for the radial positions $x/D = 1.0$ and $x/D = 2.0$ in Fig. 10 (a) and Fig. 10 (b), respectively. It is evident that an increase in the normalised roughness, h_s/D , decreases the magnitude of the maximum wind speed, u_{max} , and raises the elevation at which it occurs, z_{max} . These findings are as reported by Xu and Hangan (2008) and Choi (2004). It is however shown that the extent to which u_{max} and z_{max} change is different for the two radial positions. This flow behaviour is expected because the diverging wall jet flow is made up of a developing boundary layer in the near-wall region that will, with divergence, give mechanical

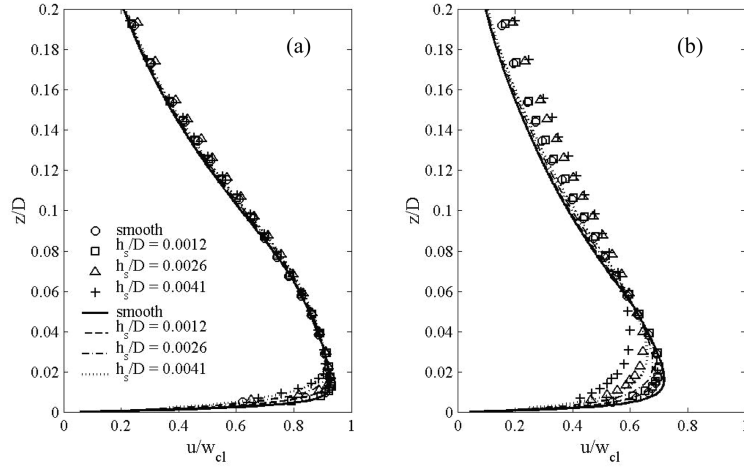


Fig. 10 Experimental and numerical normalised mean velocity profiles for smooth and rough surface tests at (a) $x/D = 1.0$, and (b) $x/D = 2.0$. Experimental results are shown as symbols, and numerical predictions are shown as lines

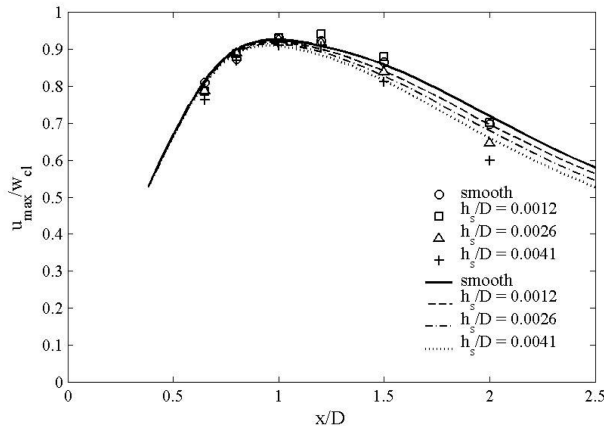


Fig. 11 Variability of the normalised velocity maxima u_{max}/w_{cl} with radial position and surface roughness. Experimental results are shown as symbols, and numerical predictions as lines

turbulence more time to influence the flow field. The observed decreasing trend in u_{max} and increasing trend in z_{max} , with respect to the smooth surface tests, will continue to occur until a balance is achieved between the wall friction and shearing of the overlying flow. This balance is expected to be at least dependent on surface roughness and jet Reynolds number. It is evident that the numerical model predicts the change in mean velocity profile at $x/D = 1.0$ very well, but under predicts the flow distortion at $x/D = 2.0$ for u_{max} , z_{max} , and δ for larger values of surface roughness.

Inspecting the decay of u_{max} with surface roughness and radial position, Fig. 11 shows that in the region near u_{storm} there is little change in the observed profile shape or magnitude. As the flow diverges, increasing surface roughness steadily decreases the magnitude of u_{max} . It was found that the offset of rough surface results from the smooth surface case settled to a constant ratio at approximately the self-similar location (Knowles and Myszkowski 1998). Experimentally it is unclear

whether similar behaviour occurs because of the small number of testing locations at larger radial positions. The location where surface roughness begins to offset u_{max} from the smooth surface tests unsurprisingly appears to be Reynolds number dependent when current results are compared with those for a higher Reynolds number jet (Xu and Hangan 2008). In these experimental results a significant offset is observed over the entire testing domain, $0.8 \leq x/D \leq 3.0$. A Reynolds number dependency is intuitively expected when considering rough wall boundary layer behaviour is controlled by the dimensionless roughness parameter $h_s^+ = u^* \cdot h_s / \nu$, where u^* is the wall friction velocity defined by $u^* = (\tau_w / \rho)^{1/2}$, which itself is dependent on Reynolds number. Therefore, although in the current simulations there is little u_{storm} dependence on surface roughness, with the massive increase in Reynolds number to a full-scale event, it may be expected that there will be noticeable influence. This implies that if accurate roughness influence simulations are to be extrapolated to full-scale events, the jet Reynolds number should be increased significantly from that used here, and the flow along the impingement surface should be classified as “fully turbulent” ($h_s^+ > 60$) (White 1991), as this will be the case for full-scale downburst events. Results in Xu and Hangan (2008) imply that a jet Reynolds number greater than approximately 1.0×10^6 is required to meet this criterion. As an example, an experimental jet diameter of 1 m and bulk outflow velocity of 15 m/s would suffice.

The numerical model appears to predict experimental variability in u_{max} well for all radial positions and surface roughness levels for $x/D \leq 1.5$, but fails to predict the drop in magnitude after this location, particularly for the two roughest simulations. At $x/D = 2.0$, Xu and Hangan (2008) report a decrease in u_{max}/w_{cl} 0.15 when comparing $h_s/D = 0.004$ with their smooth case; this is greater than the $u_{max}/w_{cl} \approx 0.1$ reduction herein for a similar level of surface roughness. It is therefore expected that the difference between the experimental and numerical results at $x/D = 2.0$ is not an error in the experimental measurements.

Inspecting the variability of z_{max} for the range of surface roughness and radial positions tested, Fig. 12, the trend of increasing z_{max} with increase in both surface roughness and radial position noted for Fig. 10 is evident. The numerical predictions show smoother trends than the experimental data, but in general agree reasonably well, particularly in light of the error scale discussion of section 3.2. The numerical predictions for z_{max} appear, at larger radial locations, to be offset from the smooth surface by a constant ratio, supporting the concept that a type of equilibrium exists once

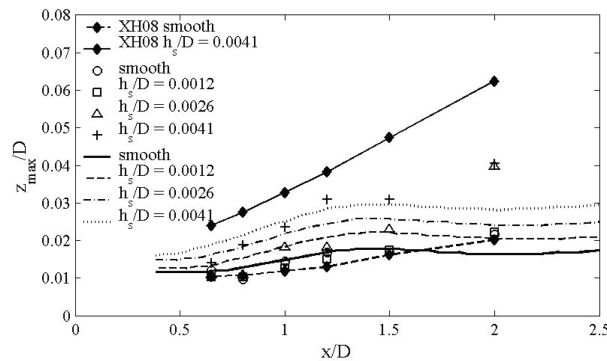


Fig. 12 Variability of the normalised elevation to velocity maxima, z_{max}/D , with radial position and surface roughness. Experimental results are shown as symbols, and numerical predictions as lines. Empirical model results of Xu and Hangan (2008), Eq. (2), are shown as filled markers joined by lines

the mechanical turbulence has established. Xu and Hangan (2008) studied the influence surface roughness, radial location and Reynolds number have on z_{max} . From these results an empirical formula for z_{max} was derived, Eq. (2), and is shown (XH08) alongside the current results in Fig. 12. The empirical equation does a good job at predicting the experimental smooth surface z_{max} values, but overestimates those both measured and numerically predicted for the rough surface case. A reasonable replication of the rough surface z_{max} shape is seen. The overestimation by the empirical model for the rough surface case is expected because the model is calibrated for local Reynolds numbers ($Re_l = x \cdot u_{max}/\nu$), $Re_l > 2.5 \times 10^5$, whereas the current test results lie in the range $4.2 \times 10^4 \leq Re_l \leq 1.0 \times 10^5$. This again highlights the Reynolds number dependence of roughness driven flow characteristics. If the empirical formulation of Xu and Hangan (2008) holds for extrapolation to full-scale downburst Reynolds numbers (and the impinging jet analogy is acceptable) this could be an extremely useful design tool.

$$\sqrt{\frac{x}{z_{max}}} = -1.95 \cdot \ln \left[\frac{h_s}{0.08D} + \frac{139}{Re_l \sqrt{2z_{max}/D}} \right] \quad (2)$$

A by-product of the surface roughness induced decrease in u_{max} , Fig. 11, is that the wall jet thickness, $\delta = z(u_{max}/2)$, is altered. Fig. 13 shows that increasing surface roughness, particularly at larger radial locations, has the influence of increasing δ . The trend seen is unsurprisingly similar, but inverted to that shown in Fig. 11 for u_{max} . The Reynolds number dependency discussed for Fig. 11 will equally apply to δ .

Figs. 14 (a) and (b) show turbulence kinetic energy profiles for $x/D = 1.0$ and 2.0 respectively, matching the mean velocity profiles shown in Fig. 10. It is evident (numerically) that at $x/D = 1.0$ only the inner region of the flow is significantly influenced by surface roughness, as was observed for the mean velocity profiles. It is seen numerically that as the surface roughness increases the amount of turbulence energy near the surface also increases; this finding agrees with the results of Xu and Hangan (2008). For $x/D = 2.0$ there appears to be profile variability in the upper region, where below the peak in k , increasing roughness tends to reduce the observed level of turbulence at

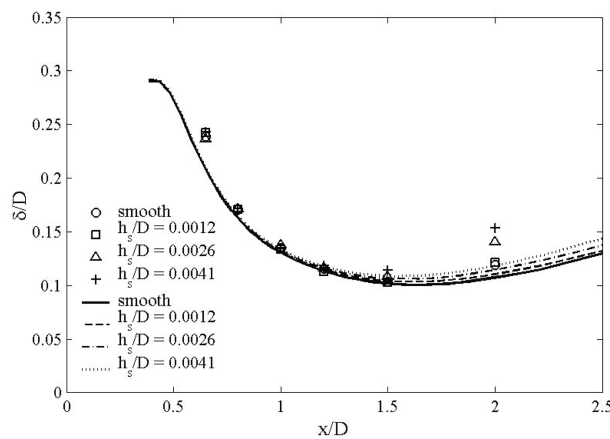


Fig. 13 Variability of the normalised wall jet thickness, δ/D , with radial position and surface roughness. Experimental results are shown as symbols, and numerical predictions as lines

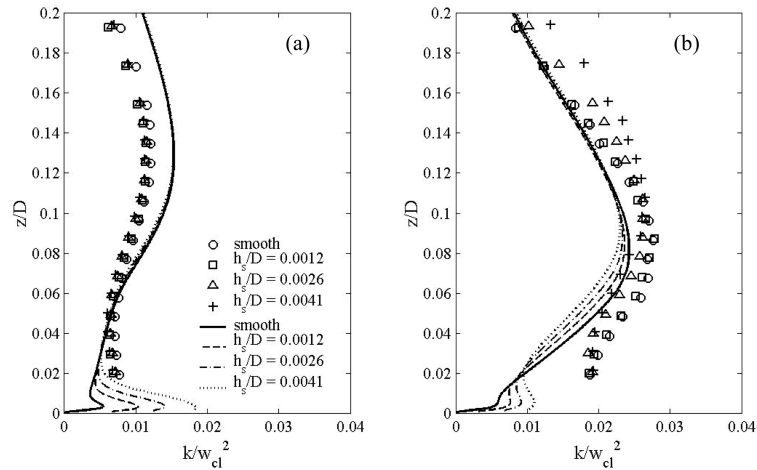


Fig. 14 Normalised turbulence kinetic energy, k , profiles at (a), $x/D = 1.0$, and (b), $x/D = 2.0$, for the range of rough surfaces tested. Experimental results are shown as symbols, and numerical predictions as lines

a given elevation, while above this point (experimentally), the turbulence is increased. These trends occur because the k profile is shifted away from the impingement surface for each increase in surface roughness. This shift corresponds to what is observed in Fig. 10 where the normalised velocity profile is lifted in this same manner. As with the normalised velocity profiles, the numerical simulation fails to predict the measured turbulence structure in the near-wall region, significantly under-estimating the turbulence magnitude. The numerical model does succeed however in predicting the upward shift in peak k and the small reduction in magnitude as measured experimentally, but fails to match these measurements above this point.

From the information presented in this section it is clear that for impinging jet simulations run at the Reynolds number described here, there is only a minor influence on the storm maximum profiles due to surface roughness. However, through comparison with the empirical model of Xu and Hangan (2008), it is evident that for higher Reynolds numbers, possibly extending to the scale of a full-scale downburst event, this may not be the case. It is therefore evident that if experimental simulations approximating downburst events are to accurately model the influence of surface roughness, a much larger scale (Reynolds number) than used in this simulation must be used.

3.4. Empirical model

Analytical and empirical models have been developed to predict downburst wind structure and its impact on aviation safety (Ivan 1986, Oseguera and Bowles 1988, Vicroy 1991, Zhu and Etkin 1985) and design of engineered structures (Chay, *et al.* 2006, Holmes and Oliver 2000, Ponte and Riera 2007, Wood, *et al.* 2001, Xu, *et al.* 2008). In this section the self-similar empirical model of Wood, *et al.* (2001) is expanded to include the influence of jet tilt and surface roughness. The model is an empirical model of a laboratory-scale steady impinging jet. However, the areas where this model is expected to be significantly different for full-scale steady impinging downburst flow are highlighted. Model development was limited to the forward side of the outflow because this is where integrated loading cases will be highest.

Wood, *et al.* (2001) proposed a simple equation describing the normalised vertical profile of

horizontal velocity for the self-similar region of a steady flowing impinging jet, Eq. (3). This equation uses the wall jet thickness variable, δ , to normalise elevations. The constants C_1 , C_2 , and C_3 can be solved by applying the boundary conditions given in Eqs. (4) - (6) and prescribing a normalised elevation of maximum velocity, z_{max}/δ . The values given in Wood, *et al.* (2001) for C_1 , C_2 , and C_3 are 1.55, 1/6 and 0.70 respectively, which correspond to $z_{max}/\delta \approx 0.18$.

$$\frac{u}{u_{max}} = C_1 \left(\frac{z}{\delta} \right)^{C_2} \left[1 - \operatorname{erf} \left(C_3 \left(\frac{z}{\delta} \right) \right) \right] \quad (3)$$

$$\frac{u}{u_{max}} = 0.5 \quad \text{for} \quad \frac{z}{\delta} = 1 \quad (4)$$

$$\frac{u}{u_{max}} = 1 \quad \text{for} \quad \frac{z}{\delta} = \frac{z_{max}}{\delta} \quad (5)$$

$$\frac{\partial(u/u_{max})}{\partial(z/\delta)} = 0 \quad \text{for} \quad \frac{z}{\delta} = \frac{z_{max}}{\delta} \quad (6)$$

The issue with applying this profile to predicting maximum downburst wind loads is that self-similarity does not occur until well after the location of maximum wind speeds. Although Knowles and Myszko (1998) show that mean velocity self-similarity does not exist until $x/D > 3$, theirs and current results show that this similarity is close to being achieved for $x/D > 1.5$. Similar findings were expressed in Wood, *et al.* (2001). It is therefore pertinent, given that maximum wind speeds occur at $x/D \approx 1$, to seek a model that better predicts the region $x/D < 1.5$ so the high wind speed region can be better predicted. The current model development aims to achieve this.

3.4.1. Model development

A primary reason why the self-similar profile is inappropriate for predicting mean velocities at $x/D < 1.5$ is because the normalised elevation of maximum velocity, z_{max}/δ , does not remain constant through this region. This is highlighted in Fig. 15 where it is evident that $x/D = 0.65$, z_{max}/δ is well below

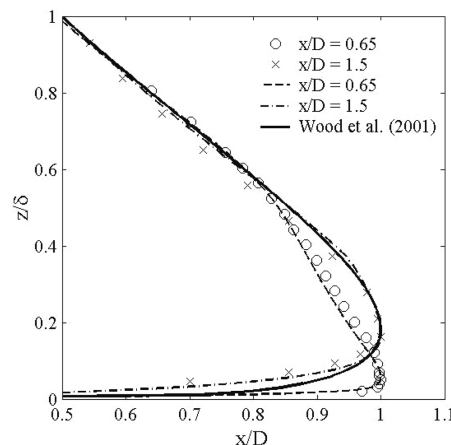


Fig. 15 Normalised experimental (symbols) and normalised simulation (dashed line) velocity profiles for $x/D = 0.65$ and $x/D = 1.5$ as compared with the empirical model of Wood, *et al.* (2001)

Wood's prescribed elevation of 0.18. As expected, the extent of model disagreement reduces as the flow approaches self similarity; this is seen by the relatively good agreement with the $x/D = 1.5$ data set.

To address this issue it is appropriate to introduce radial dependence into the normalised variable z_{max}/δ in Eqs. (5) and (6). This provision requires values of C_1 , C_2 , and C_3 to be recomputed for each radial position, allowing a more accurate prediction of the elevation of maximum velocity. Fig. 16 shows the change in z_{max}/δ with radial position for the current numerical and experimental simulations, and results from previous experimentation (Cooper, *et al.* 1993). Fig. 16 shows a fitted curve to be used in Eqs. (5) and (6) for calculating constants C_2 and C_3 . The general equation for this curve, Eq. (7), has the physical constraint of remaining approximately constant (~ 0.13) for $x/D > 3$ (Knowles and Mysko 1998), and has been fitted based on visual inspection and linear regression (as were all variables discussed in this section). It was found that the normalised elevation of maximum winds is also dependent on surface roughness and jet tilt. The influence of surface roughness has been included in Eq. (7) through the variable R , Eq. (8). For the tilted jet simulations it was found that when results were normalised against δ and u_{max} , mean velocity profiles for $x/D \geq 1.5$ collapsed to the surface normal self-similar profile. However, for the region $x/D < 1.5$, profiles display a trend towards larger z_{max}/δ values with increased angles of jet tilt. However, it was found that ignoring this dependence could generally be done without impacting profile predictions significantly.

$$\frac{z_{max}}{\delta} = \frac{R}{15} \left[2 + \exp\left(-\left[0.45\left(\frac{x}{D}\right)^4\right]\right) \right] \left[1 - \exp\left(-\left[0.95\left(\frac{x}{D}\right)^3\right]\right) \right] \quad (7)$$

$$R = 100\left(\frac{h_s}{D}\right) + 1 \quad (8)$$

Given the profiles close to the impingement region are not self-similar, it is not surprising that the profiles do not collapse to a single profile even when the elevation of maximum winds are corrected. Hence, additional profile corrections are required. The final form of the non-dimensional velocity profile equation is given in Eq. (9), and includes two additional terms, λ , and ζ ; λ is an

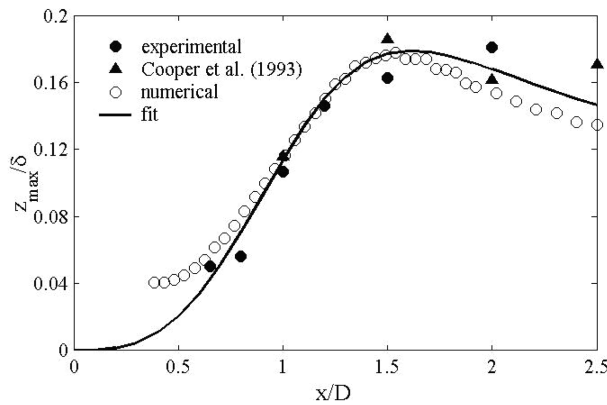


Fig. 16 Variability of the normalised elevation of maximum wind speed, z_{max}/δ , for $x/D < 2.5$

“in-boundary layer” correction, and ζ is an “out-of boundary layer” correction. The names, “in-” and “out-” of boundary layer conform to the nomenclature of Oseguera and Bowles (1988) and refer to the regions $z < z_{max}$ and $z > z_{max}$, respectively. These regions are similar to, but not exactly the same as the inner and outer layers discussed earlier. The additional terms vanish at the boundary conditions specified in Eqs. (4) - (6), and therefore have no bearing on the calculation of C_1 , C_2 or C_3 . These terms also vanish outside the in or out of boundary layer region not being corrected (i.e. $\lambda = 1$ for $z > z_{max}$ and $\zeta = 0$ for $z < z_{max}$).

$$\frac{u}{u_{max}} = C_1 \lambda \left(\frac{z}{\delta} \right)^{C_2} \left[1 - \operatorname{erf} \left(C_3 \left(\frac{z}{\delta} \right) \right) \right] + \zeta \quad (9)$$

The requirement for the in-boundary layer correction term, λ , can be seen from Fig. 15, where the original empirical model of Wood, *et al.* (2001) over-predicts both the experimental and numerical results for $x/D = 1.5$. This characteristic is evident for all radial positions when only a shift of z_{max}/δ and the corresponding changes in C_1 , C_2 and C_3 are applied. Therefore the in-boundary layer correction term takes the form:

$$\lambda = 1 - \left(\frac{1}{R} \right)^2 \left[1 - \frac{\min \left(\frac{z}{\delta}, \frac{z_{max}}{\delta} \right)}{\left(\frac{z_{max}}{\delta} \right)} \right]^8 \quad (10)$$

where the min(imum) function is used to restrict the correction to just the in-boundary layer region. Generally λ was found to be independent of radial position, jet tilt, and surface roughness. However, when both jet tilt and surface roughness were present, the inverse of the roughness parameter, $(1/R)$, is introduced to yield a better representation of experimental results.

The out-of boundary layer constant, ζ , is required primarily close to impingement, where shifting the location of z_{max}/δ leads to an underestimate of wind speeds in the region $z_{max}/\delta < z/\delta < 1$. ζ is a cosine function fit between these limits with a variable scaling factor, ψ , dependent on x/D and θ . Little dependence on surface roughness was found in ψ . Eq. (11) gives the general form of ζ .

$$\zeta = \psi \cdot \cos \left[\frac{\pi}{2} \left(\frac{\min \left(\left| \frac{z}{\delta} - z_c \right|, 1 - z_c \right)}{1 - z_c} \right) \right]^{\frac{3}{2}} \quad (11)$$

In Eq. (11), z_c is the normalised elevation of the mid-point of the region $z_{max}/\delta < z/\delta < 1$ and is calculated as:

$$z_c = \frac{\left(\frac{z_{max}}{\delta} \right) + 1}{2} \quad (12)$$

The scaling factor, ψ , is calculated by summing two components; ψ_x , based on x/D , and, ψ_θ , based on both x/D and θ , Eqs. (13) - (15). Both ψ_x and ψ_θ approach zero as the flow approaches self-similarity where the normalised velocity profile is closely approximated by the original model

formulation.

$$\psi = \psi_x + \psi_\theta \quad (13)$$

$$\psi_x = 0.065 \cdot \exp \left[- \left(2 \left(\frac{x}{D} \right) - 1 \right)^5 \right] \quad (14)$$

$$\psi_\theta = 0.1 \cdot \theta^{0.45} \cdot \exp \left[- \left(\frac{\left(\frac{x}{D} \right)^5}{(1.1 + 0.8\theta)} \right) \right] \quad (15)$$

It should be noted that ζ goes to zero at $z/\delta=1$ and no correction is applied above this point. Little attempt has been made to ensure a good fit of the empirical model in this upper region, primarily because it is of little concern when considering design strength winds (i.e. the wind speed is less than $u_{max}/2$), and in most cases this point will be located above the elevation of a structure under consideration. However, it was found that specifying a value of $z_{max}/\delta=0.12$ fits all available data reasonably well to $z/\delta=2$. It is recommended that this value be applied if this upper region is of interest.

For the model to have general applicability in predicting absolute velocity fields, the normalisation variables, u_{max} , and δ , must also be described with respect to radial position, surface roughness, and jet tilt. To enable the model to be used for both laboratory scale impinging jets and (*in theory*) full-scale downburst predictions, these variables are normalised against the jet diameter, D , and the centre line mean jet velocity, w_{cl} . Normalising variables in this manner allows the user to prescribe the desired impinging jet/downdraft size and intensity, and means that only one length-scale is required throughout the model.

It was seen in Fig. 7 that as the angle of jet tilt, θ , increased, so too did the radial location of u_{max} . This behaviour is replicated in the model formulation, Eq. (16), which is adapted from the radial velocity decay of Oseguera and Bowles (1988). As most microburst wind events are short lived, Vicroy (1991) updated the velocity decay model to better agree with full-scale observations. Despite this update the original model has been maintained because of its closer resemblance to a steady-state flow case.

$$\frac{u_{max}}{w_{cl}} = \left(\frac{u_{storm}}{w_{cl}} \right) \frac{R_u \alpha}{2\beta x_\theta} \left[1 - \exp \left[- \left(\frac{x_\theta}{\alpha} \right)^{1.9} \right] \right] \quad (16)$$

$$\alpha = 1.18\theta + 0.98 \quad (17)$$

$$x_\theta = \frac{x}{D} + \theta \quad (18)$$

$$R_u = 1 - 35 \frac{h_s}{D} \left[1 - \exp \left[- \left(\frac{1}{1.7} \left(\frac{x}{D} \right)^4 \right) \right] \right] \quad (19)$$

The ratio u_{storm}/w_{cl} is the jet centre-line normalised storm maximum velocity recorded for each smooth surface model configuration. It was found that, to within 2%, the normalised maximum storm velocity remained constant for all tilted jet simulations at $u_{storm}/w_{cl}=0.97$, a small increase on

the $u_{storm}/w_{cl} = 0.93$ observed for the $\theta = 0$ case. Jet tilt is incorporated into the original velocity decay function by the variables α , and x_θ , which artificially shift the point that u_{max} goes to zero, mimicking the results of Fig. 7. The influence of surface roughness is accounted for through the variable R_u , which decreases from a value of 1 as x/D increases, Eq. (19). The value of the constant β should be taken as 0.317. Considering the observations made in section 3.3 regarding the Reynolds number dependence of the velocity magnitude on surface roughness, the current formulation of R_u may be inappropriate for full-scale downburst applications. However, without further simulations at higher Reynolds numbers, a more appropriate formulation cannot be given.

The variation of the normalised wall jet thickness, δ/D , must also be described to remove the model dependence on this length-scale. As would be expected from Fig. 6 and Fig. 13, δ is dependent on x/D , θ , and h_s/D . The normalised wall jet thickness is described by:

$$\frac{\delta}{D} = R_\delta \left[(1 - 0.3\theta) \cdot \exp \left[- \left(2.3 - \frac{3\theta}{2} \right) \left(\frac{x}{D} \right) \right] + 0.08 \left(\frac{x}{D} \right) - 0.05 \right] \quad (20)$$

where R_δ is a surface roughness parameter that accounts for the lifting of the wall jet thickness by the surface roughness as the jet spreads radially, and is described by:

$$R_\delta = 1 + 65 \left(\frac{h_s}{D} \right) \cdot \exp \left[- \left(\frac{3}{2} \left[\frac{x}{D} - 2.2 \right] \right)^2 \right] \quad (21)$$

It is expected that this variable will again be Reynolds number dependent, and may require adjustment for full-scale application.

At full-scale, it would be more appealing to prescribe the behaviour of z_{max}/D , instead of δ/D , as this has more meaning to the scale of a structure. This would also allow use of the Reynolds number dependent empirical formulation by Xu and Hangan (2008) for surface roughness, which will be more appropriate for full-scale application than the roughness formulation here. Unfortunately without further information on the Reynolds number dependence of u_{max} and δ , Eq. (2) cannot be used in the current model. However, if it is assumed that there is no Reynolds number dependence on the influence of jet tilt, a tilt influenced magnitude of z_{max} can simply be calculated by applying a tilt multiplier, T , to the value of z_{max} calculated with Eq. (2), Eq. (22). This may have practical importance for future model developments. Considering the work of Knowles and Myszko (1998), there may be a dependence of this multiplier on the jet outlet to impingement surface distance because of the variable spread of the free jet as it moves through the air.

$$T = 1 + 13 \cdot \theta^{1.5} \cdot \exp \left[- \left(\frac{x}{D} \right)^{1.5} \right] \quad (22)$$

3.4.2. Model output

To assess the base model performance, Fig. 17 shows a normalised comparison between the model output, Eq. (9), and experimental results for the $\theta = 0$, smooth surface test for $0.65 \leq x/D \leq 2.0$. It is seen that the model generally predicts the variability in both profile shape and magnitude well. Approximations made by fitting equations to the experimental data are seen to be small, but some differences are evident. To quantify the empirical model an averaged error, \bar{E} , has been calculated for each profile, Eq. (23).

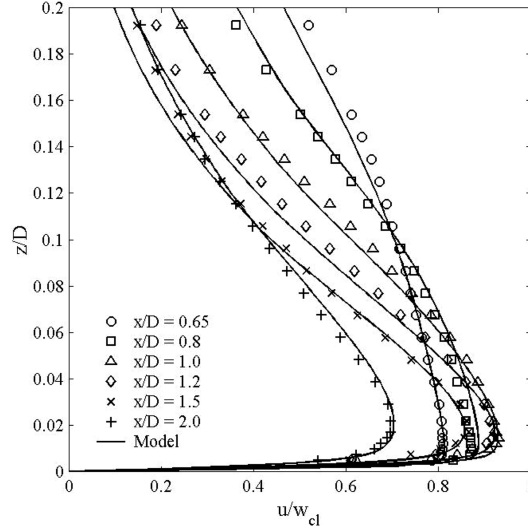


Fig. 17 Comparison between empirical model output and experimental results for the $\theta = 0$, smooth surface test case

$$\bar{E} = \frac{\sum_{i=0}^{i=n} |u_{n, model} - u_{n, exp}|}{n \cdot u_{max}} \cdot 100\% \quad (23)$$

Errors were calculated at the elevation of each experimental data point and averaged up to $z/D = 0.25$. Eq. (23) is formulated so that the profile is assessed on an absolute deviation from the experimental values so that large relative errors in regions of low velocity do not skew the error value. Assessing the averaged errors for all radial positions the worst fit, at $x/D = 1.2$, yields a result of $\bar{E} \approx 3\%$; primarily due to an under-estimation of z_{max}/δ . The largest individual point errors were found at the lowest measurement elevation where the velocity gradients were largest.

Fig. 18 compares the model output and experimental results for the range of θ tested over a smooth surface. It is evident that the model accurately predicts the change in velocity structure for each location over the range of jet tilts tested and that Eq. (16) has performed well in modelling the more gradual decay in u_{max} for increased values of θ with radial position. The model assumption that the influence of jet tilt on the elevation of z_{max}/δ was relatively minor also appears to be justified with both Figs. 18 (a) and (b) showing good agreement ($\bar{E} < 4\%$), particularly in the region near u_{max} . All other predictions yielded error of $\bar{E} < 5\%$, but for the largest tilt angle, $\theta = 0.7$, and $x/D = 0.65$, the above assumption becomes less accurate with localised errors (Eq. (23) non-averaged) of $E \approx 10\%$.

Rough surface model predictions were assessed, with model output being plotted alongside experimental results in Fig. 19. The model again does a good job at predicting the velocity structure of the impingement region, with the rising elevation, and decreasing magnitude of u_{max} associated with flow over the rougher surfaces clearly shown. Assessing the averaged errors for the two radial positions shown, a maximum error of $\bar{E} \approx 3\%$ is observed, with errors for all other locations remaining below 5%.

Given the updated empirical model was formulated based on results from the numerical and experimental tests discussed in section 3.2 and 3.3, it is unsurprising that reasonably good empirical

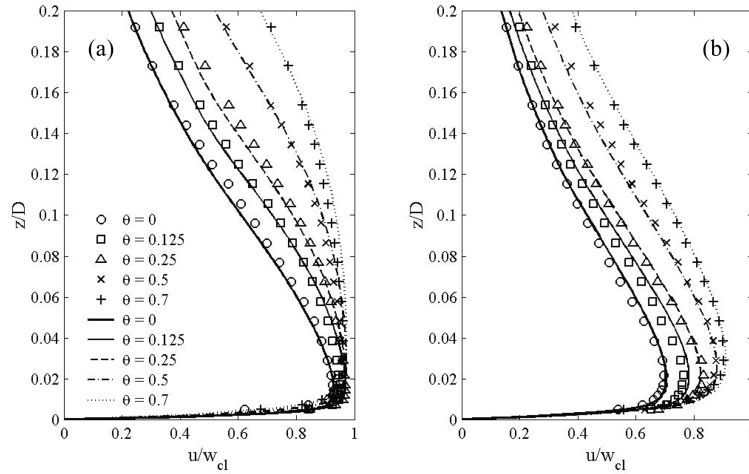


Fig. 18 Comparison between empirical model output and experimental data at (a), $x/D = 1.0$, and (b), $x/D = 2.0$, for the tilted jet cases

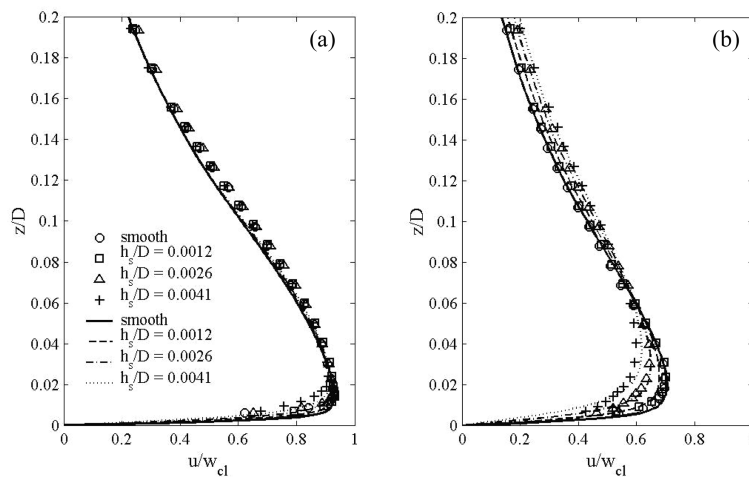


Fig. 19 Comparison between empirical model output and experimental data at (a), $x/D = 1.0$, and (b), $x/D = 2.0$, for the rough surface cases.

model predictions are found when compared with these data in isolation. More challenging is to test it against experimental results where both jet tilt and surface roughness are present, that is, data not used in the development of the model. This assessment will determine whether the dependent variables used throughout section 3.4.1 are appropriate. For this comparison, experiments were carried out for jet tilts of $\theta = 0.25$ and 0.7 with surface roughness of $h_s/D = 0.0026$ and 0.0041 . Profiles were measured at $x/D = 1.0$ and 2.0 . Empirical model predictions and experimental results are shown for these tests in Fig. 20.

Assessing the empirical model predictions for each of the test cases shown, it is evident that reasonable estimates of the velocity profile are produced. Discrepancies that do exist, are particularly prevalent for a tilt of $\theta = 0.7$ at $x/D = 2.0$, where the predicted velocity profile below

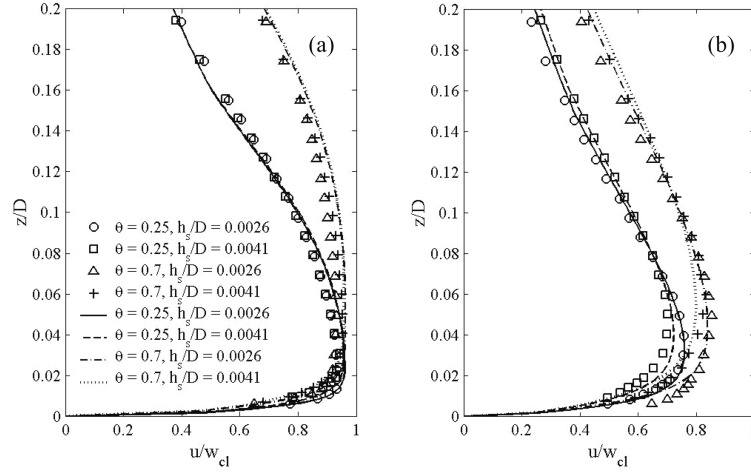


Fig. 20 Comparison between empirical model output and experimental data at (a), $x/D = 1.0$, and (b), $x/D = 2.0$, for cases where both jet tilt and rough surface are included

u_{max} appears to decrease too rapidly, i.e. an error in λ . The presented model prediction already incorporates an attempt to alleviate this issue by the inclusion of the $(1/R)$ term in Eq. (10), which makes model prediction for $x/D = 1.0$ more accurate, but fails to fully remove errors at $x/D = 2.0$. It is expected that the reason for the differing influence of surface roughness between the tilted and non-tilted cases is linked to a change in wall shear (due to differing u_{max} elevations), that is unable to be predicted by the model. Assessing the averaged error for this location reveals an error of only $\bar{E} \approx 4\%$, implying that over the entire profile the model is still doing an acceptable job. The averaged errors for all other profiles displayed range between 2% and 5%. It is therefore evident that although there is clearly some coupled behaviour between jet tilt and surface roughness, the independent models developed perform acceptably in predicting velocity structure in the impingement region.

4. Conclusions

A steady impinging air jet has been used to simulate experimentally and numerically a downdraft impinging flat ground. The influence of downdraft tilt angle and surface roughness on the ensuing wall jet velocity and turbulence characteristics have been investigated. It is believed that the principles found from these simplified tests can be applied to the more complex state of real downburst events.

For the forward side of the jet outflow, it was found that the flow depth produced by a tilted jet was deeper than for the surface-normal impinging jet and as the angle of jet tilt increased, the radial extent over which high wind speeds were measured increased. Maximum wind speeds were found to be relatively independent of jet tilt, but the radial location of these winds were found to shift away from the jet centre-line with increased tilt. The elevation of maximum wind speeds for each radial location was found to be dependent on jet tilt, but appear to be converging with divergence. However, to the rear of the jet the outflow depth decreased with increased tilt, the maximum outflow intensity was highly dependent on jet tilt, and the location of maximum winds remained relatively constant. It is therefore evident that when considering maximum potential loading within a given simulated event, tilted downbursts have the potential to cause larger structural loads than surface-normal events.

For the rough surface simulations it was found that surface roughness had the bulk characteristic of decreasing the magnitude of wind speeds at a given location and raising the elevation at which these maximum winds occur. These findings are in agreement with the work of Xu and Hangan (2008). For the current simulations it was found that the extent to which maximum wind speeds were either reduced in magnitude, or lifted from the surface, was dependent on the distance from the jet centre-line. It was found that for the region close to the impingement points ($x/D < 1.0$), surface roughness played only a minor role in determining both the velocity and turbulence structure. However, as the flow diverged, the role surface roughness played was significantly increased. This behaviour differed from the findings of Xu and Hangan (2008) for a jet of higher Reynolds number, where significant influence was found close to impingement. The difference between the current work and Xu and Hangan (2008) implies that a Reynolds number dependency exists in the flow reaction to rough surfaces. Therefore it is concluded that flow of higher jet Reynolds number than tested here may be needed to be representative of full-scale downburst flow.

The numerical model was generally found to perform well for all flows over smooth surfaces, but had difficulty predicting velocity and turbulence profiles accurately in the rough wall cases. The numerical model appears to under predict the extent to which the surface roughness influences both the velocity and turbulence profiles for $x/D > 1.5$. In the region $x/D \leq 1.5$ however the roughness formulation appears to perform relatively well when predicting velocities.

Using the results from both the jet tilt and surface roughness simulations an empirical model of the jet outflow velocity that predicted velocity profiles well for both the data it was calibrated for, and a set of bi-variate experiments was developed. It is anticipated that the formulated empirical model could be extrapolated to predict full-scale downburst winds, provided the steady impinging jet assumption for downburst flow is considered acceptable. However, it is recommended that more tests be done to determine any Reynolds number dependency on the model variables derived. This is particularly pertinent for the surface roughness terms where differences were observed between the current results and those of Xu and Hangan (2008).

References

- ANSYS (2007), *CFX 11.0*, see <http://www.ansys.com/Products/cfx.asp>.
- Chay, M.T., Albermani, F. and Wilson, R. (2006), "Numerical and analytical simulation of downburst wind loads", *Eng. Struct.*, **28**(2), 240-254.
- Chay, M.T. and Letchford, C.W. (2002), "Pressure distributions on a cube in a simulated thunderstorm downburst. Part A: stationary downburst observations", *J. Wind Eng. Ind. Aerod.*, **90**(7), 711-732.
- Choi, E.C.C. (2004), "Field measurement and experimental study of wind speed profile during thunderstorms", *J. Wind Eng. Ind. Aerod.*, **92**(3-4), 275-290.
- Cooper, D., Jackson, D.C., Launder, B.E. and Liao, G.X. (1993), "Impinging jet studies for turbulence model assessment—I. Flow-field experiments", *Int. J. Heat Mass Tran.*, **36**(10), 2675-2684.
- Fujita, T.T. (1983), *Andrews AFB Microburst*, SMRP Research Paper 205, Chicago.
- Fujita, T.T. (1985), *The Downburst: Microburst and Macroburst*, Satellite and Mesometeorology Research Project (SMRP) 210, Chicago.
- Fujita, T.T. (1990), "Downbursts: meteorological features and wind field characteristics", *J. Wind Eng. Ind. Aerod.*, **36**(1-3), 75-86.
- Gomes, L. and Vickery, B.J. (1976), *On thunderstorm wind gusts in Australia*, Civil Engineering Transactions, Institute of Engineers Australia, **18**, 33-39.
- Hjelmfelt, M.R. (1988), "Structure and life cycle of microburst outflows observed in Colorado", *J. Appl. Meteorol.*, **27**(8), 900-927.
- Holmes, J.D. (2002), "A re-analysis of recorded extreme wind speeds in Region A", *Australian Journal of*

- Structural Engineering*, **4**(1), 29-40.
- Holmes, J.D. and Oliver, S.E. (2000), "An empirical model of a downburst", *Eng. Struct.*, **22**(9), 1167-1172.
- Holmes, J.D., Hangan, H., Schroeder, J.L., Letchford, C.W. and Orwig, K.D. (2008), "A forensic study of the Lubbock-Reese downdraft of 2002", *Wind Struct.*, **11**(2), 137-152.
- International Organisation for Standardization (1998), *ISO 6344-1:1988(E) Coated Abrasives - Grain size analysis - Part 1: Grain size distribution test*, International Organisation for Standardization, Geneva, Switzerland.
- Ivan, M. (1986), "A ring-vortex downburst model for flight simulations", *J. Aircraft*, **23**(3), 232-236.
- Knowles, K. and Myszko, M. (1998), "Turbulence measurements in radial wall-jets", *Exp. Therm. Fluid Sci.*, **17**(1-2), 71-78.
- Laufer, J. (1954), *The structure of turbulence in fully developed pipe flow*, National Advisory committee for Aeronautics 1174, Washington.
- Letchford, C.W., Mans, C. and Chay, M.T. (2002), "Thunderstorms--their importance in wind engineering (a case for the next generation wind tunnel)", *J. Wind Eng. Ind. Aerod.*, **90**(12-15), 1415-1433.
- Mason, M.S. and Wood, G.S. (2005), "Influence of jet inclination on structural loading in an experimentally simulated microburst", *5th Asia-Pacific Conf. on Wind Engineering*, Seoul, South Korea.
- Mason, M.S., Wood, G.S. and Fletcher, D.F. (2007), "Impinging jet simulation of stationary downburst flow over topography", *Wind Struct.*, **10**(5), 25.
- Mason, M.S. (2009), "Simulation of downburst wind fields", PhD Dissertation, University of Sydney, Sydney, Australia.
- Mousley, P. (2002), *TFI Probe User's Guide*, see www.turbulentflow.com.au.
- Orwig, K.D. and Schroeder, J.L. (2007), "Near-surface wind characteristics of extreme thunderstorm outflows", *J. Wind Eng. Ind. Aerod.*, **95**(7), 565-584.
- Oseguera, R.M. and Bowles, R.L. (1988), *A simple, analytic 3-dimensional downburst model based on boundary layer stagnation flow*, NASA Technical Memorandum 100632.
- Ponte, J. Jr. and Riera, J.D. (2007), "Wind velocity field during thunderstorms", *Wind Struct.*, **10**(3), 287-300.
- Proctor, F.H. (1988), "Numerical simulations of an isolated microburst. Part I: Dynamics and structure", *J. Atmos. Sci.*, **45**(21), 3137-3160.
- Proctor, F.H. (1993), "Case study of a low-reflectivity pulsating microburst: numerical simulation of the Denver, 8 July 1989, storm", *17th Conf. on Severe Local Storms*, St. Louis, Missouri, 4-8 October.
- Sengupta, A. and Sarkar, P.P. (2008), "Experimental measurement and numerical simulation of an impinging jet with application to thunderstorm microburst winds", *J. Wind Eng. Ind. Aerod.*, **96**(3), 345-365.
- Twisdale, L.A. and Vickery, P.J. (1992), "Research on thunderstorm wind design parameters", *J. Wind Eng. Ind. Aerod.*, **41**(1-3), 545-556.
- Vicroy, D.D. (1991), *A simple, analytical, axisymmetric microburst model for downdraft estimation*, NASA Technical Memorandum 104053.
- White, F.M. (1991), *Viscous Fluid Flow*, McGraw-Hill.
- Whittingham, H.E. (1964), *Extreme wind gusts in Australia*, Commonwealth Bureau of Meteorology Bulletin 46.
- Wilson, J.W., Roberts, R.D., Kessinger, C. and McCarthy, J. (1984), "Microburst wind structure and evaluation of Doppler radar for airport wind shear detection", *J. Appl. Meteorol.*, **23**(6), 898-915.
- Wood, G.S., Kwok, K.C.S., Motteram, N.A. and Fletcher, D.F. (2001), "Physical and numerical modelling of thunderstorm downbursts", *J. Wind Eng. Ind. Aerod.*, **89**(6), 535-552.
- Xu, Z. and Hangan, H. (2008), "Scale, boundary and inlet condition effects on impinging jets", *J. Wind Eng. Ind. Aerod.*, **96**(12), 2383-2403.
- Xu, Z., Hangan, H. and Yu, P. (2008), "Analytical solutions for a family of Gaussian impinging jets", *J. Appl. Mech.*, **75**(2), 021019.
- Zhu, S. and Etkin, B. (1985), "Model of wind field in a downburst", *J. Aircraft*, **22**(7), 595-601.